Beam Steering, Beam Shaping, and Intensity Modulation Based on VCSEL Photonics

Fumio Koyama, *Fellow, IEEE*, and Xiaodong Gu, *Student Member, IEEE*

(Invited Paper)

Abstract—**A beam-steering device has been a key element for various sensing and imaging applications. We proposed a beam-steering device based on a vertical-cavity surface-emitting laser (VCSEL)-based waveguide structure. We show a giant steering angle and ultrahigh steering resolution at the same time by increasing the length of a device. In this paper, we present our high-resolution beam-steering concept based on VCSEL photonics. A steering angle of over 60° and a number of resolution points over 1000 are demonstrated for millimeter-scale devices, which is the highest in nonmechanical beam-steering devices. We also demonstrate the on-chip integration of a beam-steering function with a VCSEL. In addition, we demonstrate additional functionalities including the creation of vortex beams and low-voltage amplitude modulation with beam steering.**

Index Terms—**Beam steering, Bragg reflector, diffraction element, laser radar, light detection and ranging (LIDAR), modulator, phased array, slow light, vertical-cavity surface-emitting laser (VCSEL), vortex beam.**

I. INTRODUCTION

BEAM steering has been a key function for various sensing and imaging applications, such as projection displays, laser printers, and light detection and ranging (LIDAR) systems. Mechanical beam-steering devices such as polygonal mirror scanners have been widely used because of their wide deflection angle operations with high resolutions [1]–[4]. However, they are bulky and their beam-steering speed is limited because of their moving parts. A nonmechanical beam-steering approach is useful for various applications where the beam direction changes rapidly to random locations or when a system needs to be compact with good mechanical stabilities.

Various approaches for nonmechanical beam steering have been reported [5]–[21], which include an optical phased array, a

liquid crystal phase modulator, an electro-optic crystal deflector, an in-plane laser array, a photonic crystal laser, a phase-locked vertical-cavity surface-emitting laser (VCSEL), and so on. The beam-steering performance can be figured by a number of resolution points N, which is defined as distinguishable spot counts in far-field patterns. The N for mechanical deflectors can be larger than 1000 for practical application. It has been difficult to get a number of resolution points over 100 for nonmechanical beam-steering techniques. An optical phased array has been an interesting approach for realizing high-resolution beam steering [5], [18]–[21]. The recent Si-photonics approach enables compact 2-D beam scanners [20]. However, it has been difficult in increasing the interelements in the array for increasing N and there is a limitation in free spectrum range (FSR) of operating wavelengths. Therefore, there is a strong demand for a compact and high-resolution beam-steering device, which can exhibit a large beam-steering angle and a small divergence angle at the same time.

We proposed a high-resolution beam-steering device based on a slow-light Bragg waveguide [22]. The structure is the same as that of VCSELs [23]. The scheme as a dispersive element is similar to a virtually imaged phased array (VIPA) [24] but in a different structure with a vertical microcavity. Beam steering can be obtained in such a dispersive element with wavelength tuning. We demonstrated a high-resolution beam-steering device with N of over 1000 for a few mm-long devices [25]–[28]. A unique feature is its large angular dispersion of 1–2 °/nm, which is an order larger than a conventional diffraction grating [29] and several times larger than that of VIPA [24]. Also, the FSR is over 100 nm, thanks to its vertical microcavity.

In this paper, we present the structure, the operating principle, and the beam-steering characteristics of beam-steering devices composed of a Bragg reflector waveguide in a passive or active fashion. We realize a beam-steering angle over 60° and a number of resolution points over 1000, which is the record data in nonmechanical beam-steering devices. In addition, we discuss some future prospects of on-chip integration with a VCSEL. We demonstrate the on-chip beam steering based on a Bragg reflector waveguide laterally integrated with a VCSEL [30]. We also show additional functionalities of the creation of vortex beams and the amplitude modulation with beam steering.

II. LARGE ANGULAR DISPERSION IN A BRAGG REFLECTOR WAVEGUIDE

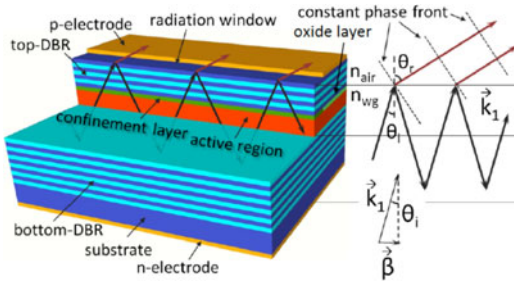A schematic structure of our beam-steering device is shown in Fig. 1. The structure in the vertical direction is the same as a

Fig. 1. Schematic cross-sectional view of a VCSEL-based beam-steering device with a Bragg reflector waveguide.
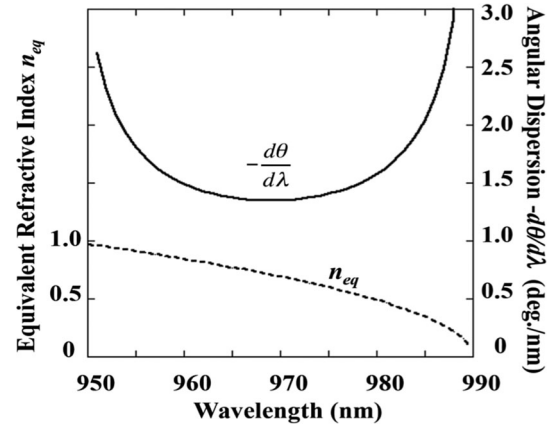
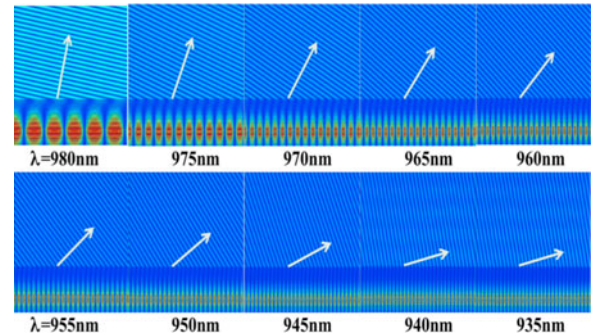

Fig. 2. Calculated dispersion of an equivalent refractive index and angular dispersion.

Fig. 3. Spatial amplitude distributions of an electric field by coupling light with different wavelengths.

conventional 980-nm VCSEL. An active region (QWs) is sandwiched by two distributed Bragg reflectors (DBRs). This waveguide structure is the so-called Bragg reflector waveguide [31]. We see large waveguide dispersion in Bragg reflector waveguides [32], resulting in slowing light [33]. Slowing light is an interesting phenomenon that reveals a new route to control light [34]–[36]. It can enable a strong light–matter interaction and introduce larger nonlinearity as well as large dispersion. In recently years, slow light has been attracting much interest for building optical functional devices such as tunable optical delay lines, switches, modulators, and amplifiers in different types of waveguides [37]–[39]. Here, we focus on a high-resolution beam steering based on a slow-light Bragg reflector waveguide [22].

If we excite a slow-light mode along the Bragg reflector waveguide, a beam of high spatial coherency can be obtained from the waveguide surface as shown in Fig. 1. This output would be similar to a VIPA [24], which provides large angular dispersion. In Fig. 1, we illustrate the device cross-sectional layer design and an excited slow-light mode in simulation. The number of DBR pairs can be designed to precisely control the mirror reflectance and, hence, the propagation loss. Here, the numbers of pairs are 28 and 40 for top and bottom DBRs, respectively. Single-mode propagation is possible when a lateral oxide-confinement aperture is narrow enough. The top-mirror reflectivity, which depends on the number of DBR pairs, is important to increase the effective radiation length. The bottom mirror is composed of 40 pairs of GaAs/AlAs DBR, providing full reflection. Electrodes are placed for current injection to the amplifier. The oxidization confinement layer is designed to guide the light mode laterally. The radiation through the top mirror results in a decay of slow-light intensity distribution. The loss can be compensated by adding gain in the active region with current injection. By adjusting the injecting current, we expect to get a near-uniform distribution of the radiation along the propagation direction.

The angle of radiation, which is called a deflection angle θ_r, is determined by the mode traveling angle θ_i as shown in Fig. 1 following Snell's Law. It is noted that the slow-light mode propagation constant β is determined by the vector numbers of waveguide cut-off condition κ_c and input light k_1, which are approximately expressed by $2\pi n_{\mathrm{wg}}/\lambda_c$ and $2\pi n_{\mathrm{wg}}/\lambda$, respectively, where n_{wg} and λ_c are the refractive index and the cut-off wavelength of the waveguide. From $k_1^2 = \beta^2 + \kappa_c^2$, β is strongly dependent on the wavelength near the cut-off condition. Therefore, by tuning the input wavelength, we are able to steer the

radiation beam. It is noted that β is highly dispersive in a Bragg reflector waveguide [32]. As a result, a large change in a deflection angle can be obtained with tuning the wavelength or tuning the refractive index of the waveguide material. By replacing the DBRs by perfect electric conductor walls for the TE mode [22], [40], [43], the equivalent refractive index n_{eq} ($=\beta \times \lambda/2\pi$) and the deflection angle θ_r are approximately given by

$$n_{\mathrm{eq}} = \sin\theta_r = n_{\mathrm{wg}} \times \sqrt{1 - \left(\frac{\lambda}{\lambda_c}\right)^2}. \qquad (1)$$

The waveguide material refractive index n_{wg} is around 3.5 for 980-nm light and has small dispersion. Fig. 2 shows the calculated dispersion of the equivalent refractive index. Large dispersion can be seen especially near the cut-off condition. Therefore, we realize beam steering of the radiated light if we tune the incident light wavelength. The calculated angular dispersion $-d\theta/d\lambda$ is also plotted in Fig. 2, which is an order of magnitude larger than conventional diffraction grating. We carried out a full-vectorial numerical simulation on the radiation field from the slow-light amplifier using a film-mode-matching method [41] (FIMMWAVE, Photon Design Co.) applying a simulation structure more close to the real one. The calculated amplitudes of electric fields for a TE-mode input are shown in Fig. 3 for different wavelengths. The deflection angle is strongly dependent on the wavelength. We can see from this graphical view
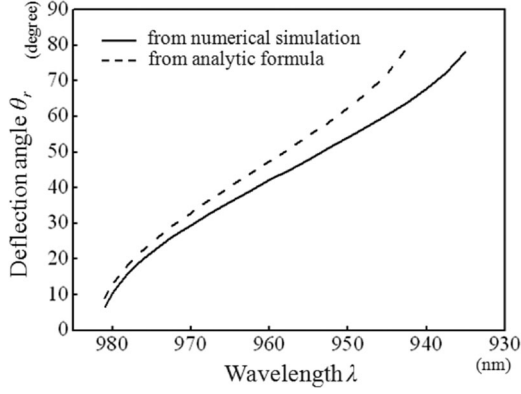
Fig. 4. Deflection angle for different wavelengths obtained from numerical simulation and analytic formula [22].

Fig. 5. Divergence angle θ_{div} and the number of resolution points N as a function of the effective propagation length L_{eff}.

Fig. 6. Schematic view of the active-type device and top view of a 1-mm-long fabricated device.

that the deflection angle increases when λ is tuned away from λ_c. At the same time, we are able to observe very clear parallel lines, which indicate the constant phase front of the radiation beam.

The calculated deflection angle in the analytic form in (1) is illustrated as the dashed line in Fig. 4 [22]. The analytical calculation is an approximation neglecting the field penetration in DBRs. The result from the simulator is also illustrated in Fig. 4 by the solid line. The curve is similar to that from the analytic formula. The maximum deflection angle can be larger than 80° for wavelength tuning of over 50 nm from the cut-off wavelength. It is important to investigate the steering resolution. The number of resolution points N, which is defined as the ratio of the maximum deflection angle $\theta_{r\,\mathrm{max}}$ and a divergence angle θ_{div}, is used to evaluate the figure of merits in beam steering. Therefore, in addition to the maximum deflection angle $\theta_{r\,\mathrm{max}}$, a beam divergence angle θ_{div} is another important factor. The radiation emitting from the waveguide surface is highly coherent and the intensity decays exponentially due to a propagation loss. The divergence angle θ_{div} is inversely proportional to the effective propagation length L_{eff} (1/e decay length) according to the diffraction limit. If the waveguide length is infinite, the diffraction pattern of the radiated intensity $I(\Delta\theta)$ is expressed by a Lorentzian function given by

$$I(\Delta\theta) \propto \frac{1}{1 + \left(4\pi \frac{L_{\mathrm{eff}} \cos\theta_r}{\lambda} \cdot \Delta\theta\right)}. \quad (2)$$

Here, $\Delta\theta$ denotes the deviation angle from the peak. Thus, the divergence angle is inversely proportional to the effective propagation length L_{eff}. Fig. 5 shows the calculated divergence angle (full width at half-maximum, FWHM) and the number of resolution points as a function of the effective propagation length for different maximum steering ranges. The effective length can be increased by reducing the propagation loss; thus, it is possible to obtain a very small divergence angle by keeping a large tunable steering range. We expect super-high-resolution beam steering with N over 1000 for 1-mm-long devices. More accurate values can be given by applying the Fourier transform of the radiation profile on the finite waveguide surface as discussed in a phase-locked VCSEL array [42].
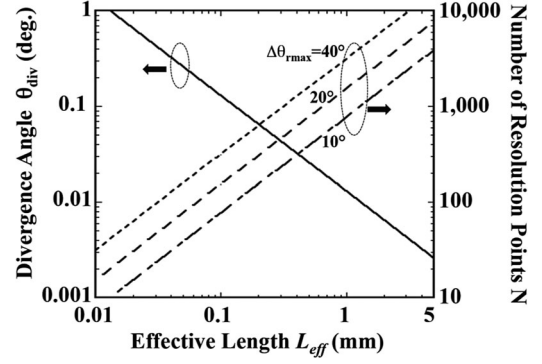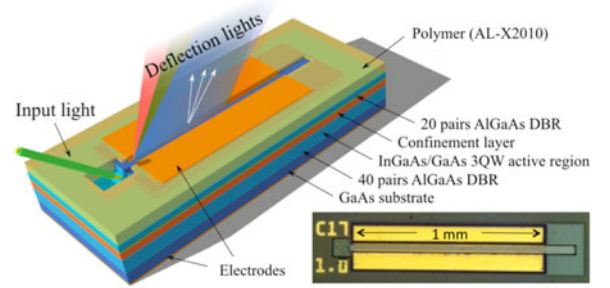
III. BEAM-STEERING EXPERIMENT

A. Active Beam-Steering Devices

We fabricated an active-type Bragg reflector waveguide [25], [26]. The device structure is illustrated in Fig. 6. In order to excite a slow-light mode, we used a tilt-coupling scheme through a lensed fiber [33]. The device is fabricated on a wafer grown by metal organic chemical vapor deposition (MOCVD). The active region contains three 980-nm-band GaInAs/GaAs quantum wells (3QWs). We carried out two times inductively coupled plasma (ICP) etching process to form the waveguide structure and fiber coupling region with different etching depths. The numbers of DBR pairs for the top mirror and bottom mirror are 20 and 40, respectively. First, ICP etches until the bottom mirror, while the second time ICP left nine pairs of a top DBR in order to get a high coupling efficiency. Then, p- and n-type electrodes are formed on both sides of the wafer. In Fig. 6, we show the top view of a fabricated 1-mm-long device.

A charge-coupled device camera is set above the device for capturing the far-field patterns (FFPs) and the near-field patterns (NFPs) at the same time. We measured the device with 50-mA current injection. Fig. 7(a) and (b) shows the FFP images and intensity profiles, respectively. Continuous deflection angle change for input wavelengths of 961–976 nm is obtained. The angle shifts over 20°. The divergence angle (FWHM) in the orthogonal direction is 10°, which is determined by the lateral spot size of an oxide-confined waveguide. The intensities at each wavelength are individually normalized by their peak intensities. We need to refrain from lasing in this VCSEL-like device,
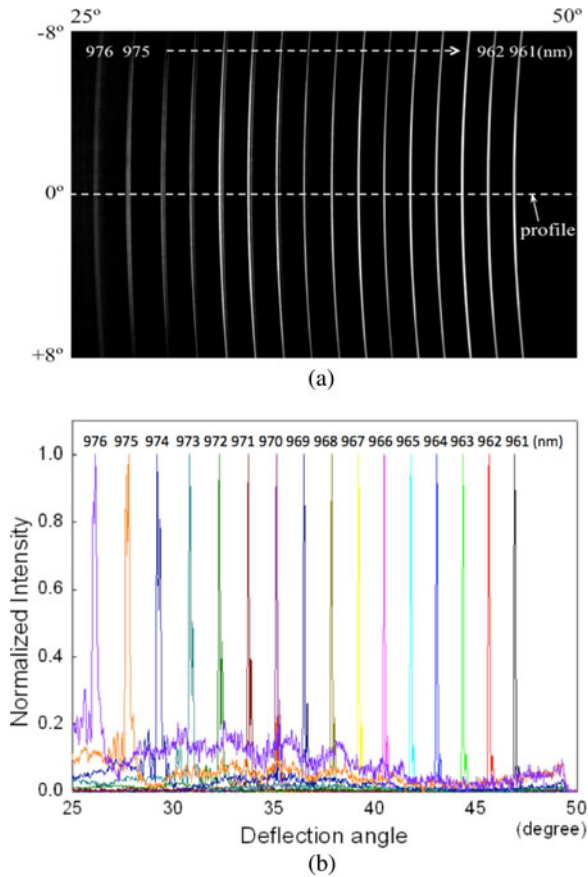
Fig. 7. (a) FFP images for different wavelengths from 961 to 976 nm in a 1-nm step. The injection current to the device is 50 mA. (b) FFP profiles for different wavelengths [43].
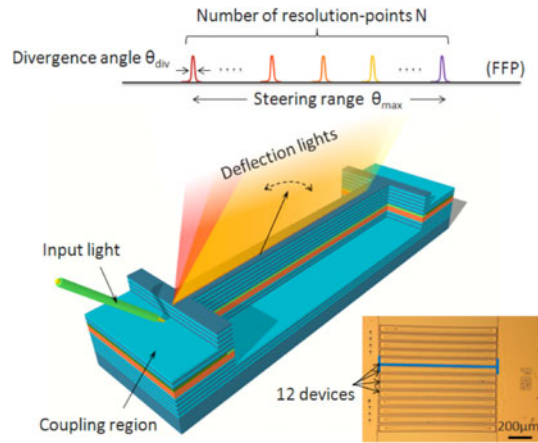

Fig. 8. Schematic view of the passive-type device and top view of a 1-mm-long fabricated array device [28].
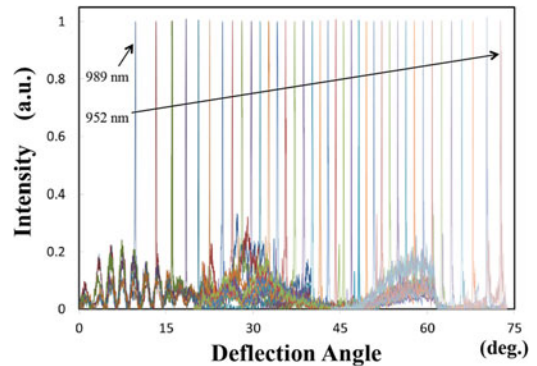

Fig. 9. Measured FFP profiles for a wavelength span of 989–952 nm with a step of 1 nm.
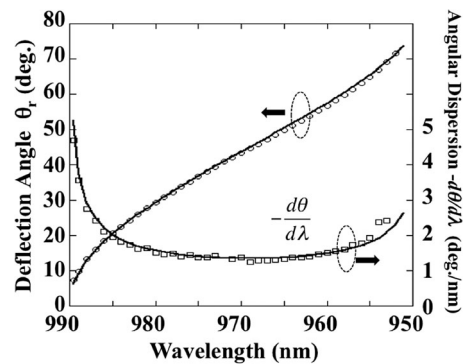
Fig. 10. Measured deflection angle and angular dispersion as a function of wavelength. Solid lines show the modeling result.

because a stimulated emission will deplete the active gain. At the moment, a lateral lasing happens first; thus, we need to design an absorption region or antireflection coating at the end of the waveguide, if we wish to pump harder. Alternatively, we are also able to design passive waveguides with extremely low propagation loss in order to get a sharper FFP profile. We fixed the polarization state of a TE mode in the present experiment.

The coupling efficiency from a fiber to slow-light mode is larger than 10 dB. It is because the input fiber position and the input angle are fixed and optimized for shorter wavelengths. In simulation, 2 dB coupling efficiency can be obtained optimally [22]. Experimental demonstration was reported previously in a similar device [33].

B. Passive Beam-Steering Devices

For higher resolutions, we designed and fabricated a low-loss passive-type device as shown in Fig. 8 [28]. The active region was replaced by a transparent bulk GaAs core, and the DBR multilayers are undoped for reducing the material absorption. The pair numbers for the top DBR and the bottom DBR are 28 and 40, respectively. As a result, the slow-light propagation loss is dramatically reduced, and hence, the effective propagation length is increased for a wide wavelength range. This fact results in an ultralow output divergence angle. Fig. 9 shows

the measured FFP profiles for a wavelength range from 952 to 989 nm for a TE mode input. The intensities are also individually normalized. The length of the measured device is 5 mm. The cut-off wavelength λ_c in this passive-type device is 990 nm, which is about 8 nm longer than that of the active-type device, so the deflection angles are correspondingly shifted. Fig. 10 shows the measured deflection angle versus wavelength together with a numerical simulation result. We could get continuous beam steering with a steering range of over $60°$. The result well agrees

Fig. 11. FFP profile captured with a high-resolution measurement system. The input wavelength is 972 nm and the polarization state is TE. The divergence angle θ_{div} is defined as FWHM.
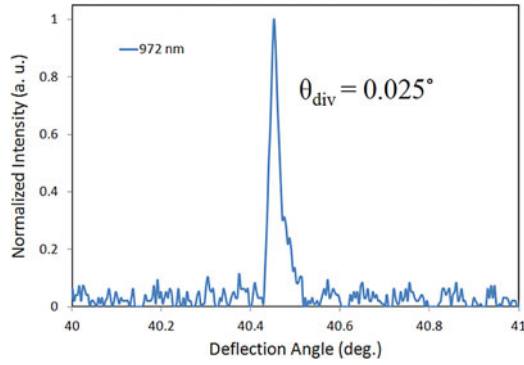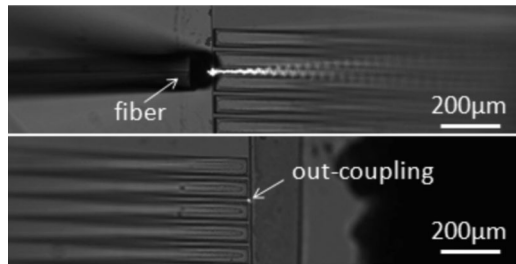

Fig. 12. NFPs captured during measurement: the top figure at the start point of a 5-mm device, the bottom figure at the end of a 5-mm device. Blurring in the images is caused by defocusing of the camera when observing at a tilt angle.
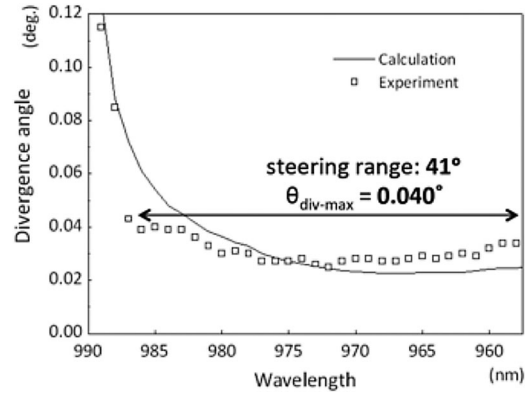

Fig. 13. Calculation and measured results of a divergence angle as a function of wavelength.

Fig. 14. Comparison between different dispersion components.

with the numerical simulation, which also shows a large angular dispersion of below $-1.5\,°/\text{nm}$.

A higher resolution measurement setup with a resolution of below $0.004°$ incorporating with a collimator is used. Fig. 11 shows the magnified FFP profile of a single-spectral line at 972 nm. Its FWHM is as narrow as $0.025°$. Some tails are found beside the main peaks. They are caused by the interference between the output radiation and the reflection light at an input. Fig. 12 shows the measured NFPs. The camera angle α is set to be $30°$ in order to capture the radiation beam. Due to the defocusing effect, we need to adjust the focus for observations at different positions of a 5-mm-long waveguide. The top and the bottom in Fig. 12(a) and (b) show the input and the end position for a 5-mm-long device, respectively. Although radiation intensity decreases with propagation, we can clearly observe out-coupling at the end of the device. The $1/e$ attenuation gives an estimation of a propagation length of 2–3 mm.

The measured divergence angles as a function of wavelengths are shown in Fig. 13 in comparison with the calculation by Fourier transform of the radiation profile on the waveguide surface. In the modeling, the propagation loss is determined by the radiation through a top DBR. Both are almost in agreement with each other. For a tuning range of 28 nm (958–986 nm), the measured divergence could be below $0.040°$. Considering the corresponding steering range of $41°$ in the entire tuning range, we achieved a record number of resolution points N larger than 1000. Further improvements can be made after reducing the propagation loss and increasing the device length.

The number of resolution points in beam steering with various dispersion elements is summarized in Fig. 14 [43]. If we look at the maximum steering angle $\Delta\theta$, which is the product of angular dispersion $d\theta/d\lambda$ and optical bandwidth $\Delta\lambda$, our device shows distinguished performances over other types of dispersion elements. Diffraction grating has $d\theta/d\lambda$ of smaller than $0.05°/\text{nm}$, and hence $\Delta\theta$ is limited. For VIPA, $d\theta/d\lambda$ can be increased by a factor of over 10, but $\Delta\lambda$ is strictly limited by its small FSR. We could see that our device has $d\theta/d\lambda$ of $1–2\,°/\text{nm}$, doubling that of VIPA. In addition, due to its large FSR of over 100 nm, $\Delta\theta$ is determined by the tuning range of input light. We expect a number of resolution points over a few thousands for an extended device to super-high-resolution beam steering.

Instead of wavelength-tuned beam steering, it is also interesting to offer beam steering at a fixed wavelength. We can do that because the deflection angle of the radiation beam is dependent on the waveguide refractive index, which is in a linear relationship with temperature. We demonstrated a beam-steering device operated by both direct heating and electrothermal heating. The device is similar to that in Fig. 7. A change larger than $7°$ in the deflection angle was obtained for temperature changes of 60 K. We also carried out electrothermal steering. The temperature increase is induced by pumping the amplifier harder. By electrical pumping of 400 mA for a 1-mm-long amplifier waveguide, we obtained over $6°$ steering in the deflection angle.
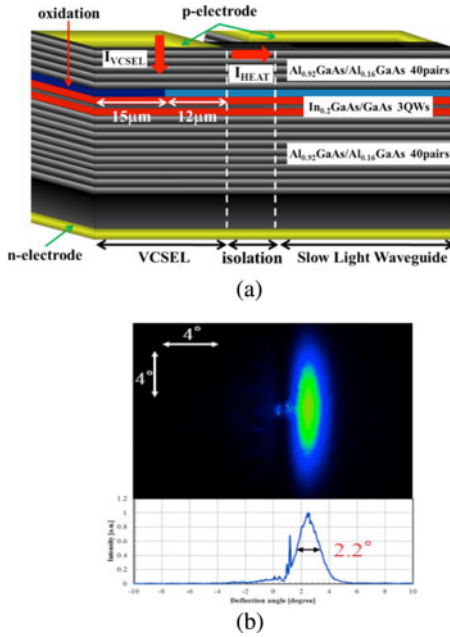
Fig. 15.   (a) Schematic structure of an on-chip beam-steering device integrated with a VCSEL and (b) FFP [45].

Integrating microheaters is our next goal. We believe that a larger steering ability can be achieved and a higher tuning efficiency is expected.

IV. ON-CHIP BEAM SCANNER INTEGRATED WITH VCSEL

We fabricate a VCSEL-based on-chip beam scanner involving a 980-nm VCSEL with a laterally coupled slow-light Bragg reflector waveguide [45]. The schematic structure of an integrated device with 980-nm InGaAs VCSEL and a laterally coupled slow-light waveguide [44] is shown in Fig. 15(a). The fabricated device consists of 25-pair $Al_{0.16}Ga_{0.84}As/Al_{0.92}Ga_{0.08}As$ top DBR, 40-pair bottom DBR, and λ-cavity containing three $In_{0.2}Ga_{0.8}As$ MQWs. The vertical emission of the VCSEL is inhibited by covering with a top Au electrode. The active region of a VCSEL and the lateral confinement of a slow waveguide are defined by an oxide-confinement structure. A VCSEL and a slow-light waveguide are directly coupled without inserting an oxidation layer in between. The gain region of the VCSEL is 12 μm $\times$ 12 μm. We formed additional electrode on a slow-light waveguide for electrothermal tuning of the refractive index of the slow-light waveguide. The spacing between the top electrodes of the VCSEL and the slow-light waveguide is 40 μm. The fabrication process is the same as conventional VCSELs.

Fig. 15(b) shows the measured FFP when an injection current into VCSEL is 6.8 mA. We can see the lateral optical excitation of a slow-light mode from a VCSEL to a Bragg reflector waveguide. According to the propagation length (20 μm) observed in NFP, we estimate a divergence angle of 2.4°, which is in agreement of a measured value in the FFP. This indicates that the radiated field from the Bragg reflector waveguide is diffraction limited. We form an on-chip heater between the two top electrodes by controlling the surface current (I_{HEAT}). When
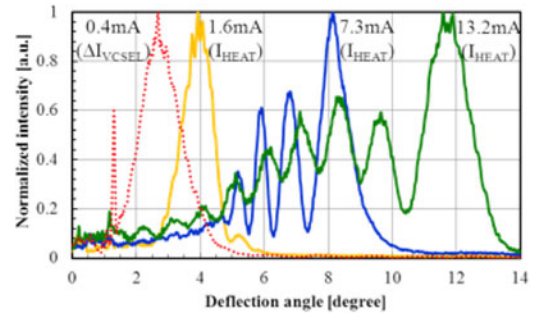

Fig. 16.   FFPs controlled by currents in a VCSEL and an on-chip heater [45].

we increase I_{HEAT}, the waveguide is heated up and λ_c is larger and hence the deflection angle is increased. On the other hand, if we keep λ_c constant while thermally changing the lasing wavelength by increasing the VCSEL current, the deflection angle can be decreased. Fig. 16 shows the measured FFPs for various I_{HEAT}. We obtained thermal continuous beam steering over 9°. From the experiment, we estimate a local temperature change of approximately 50 K. The number of resolution points, which is defined by the ratio of beam-steering range and divergence angle, is limited below 4 in the present device. We see the noticeable broadening and multiple peaks in FFPs by increasing I_{HEAT} in Fig. 16. These side lobes would be due to the interference between the radiation from the slow-light waveguide and the scattering light from the edge of the VCSEL, which should be avoided to improve the resolution. We expect a much larger number of resolution points over 100 by increasing the propagation length over 500 μm in the Bragg reflector waveguide, which could be realized by increasing an injection current in the waveguide to compensate a propagation loss.

Another possibility for on-chip beam scanners is to integrate a slow-light amplifier and a tunable MEMS VCSEL [46] with a lateral optical coupling scheme as shown in Fig. 17(a) [47]. It is composed of a Bragg-reflector-based slow-light semiconductor optical amplifier (SOA) and a cantilever-type microelectromechanical (MEMS) VCSEL [47]. The layer structure is similar to the MEMS VCSEL including an active layer; an oxide-confinement layer and variable air gap are sandwiched by top and bottom DBRs. The top-DBR mirror is freely suspended and can be actuated mechanically, which leads to the wide tunable operation as in tunable MEMS VCSELs. On the other hand, the top DBR of the slow-light SOA is fixed. There is a tapered transition region between the VCSEL and the SOA, which changes the air gap linearly. In the VCSEL section and the taper section, vertical radiation is suppressed by a 40-pair top mirror whose reflectivity is nearly 100%. The slow-light propagation mode in the SOA can be excited directly from the MEMS VCSEL as presented in the previous section. The taper transition section changes the propagation constant of a slow-light propagation mode adiabatically. Optical output is taken from the surface of the slow-light SOA section by reducing its top DBR's pair.

The coherent beam is radiated from the surface of the SOA, and it forms constant phase fronts. The deflection angle can be widely changed by means of sweeping the lasing wavelength near the cut-off wavelength of a slow-light waveguide because
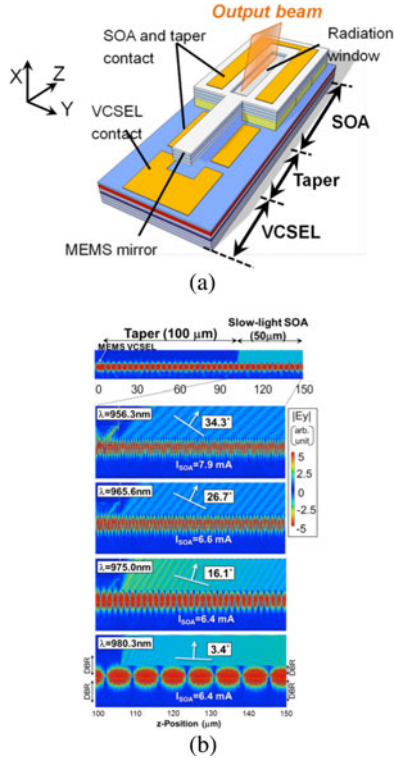
Fig. 17. (a) Schematic structure of an integrated beam scanner with a tunable MEMS VCSEL and contour plot of an electric field amplitude distribution with wavelength tuning [47].

Fig. 18. (a) Schematic structure of an integrated optical vortex beam emitter. (b) Measured field pattern for a 50-μm ring Bragg reflector waveguide.

the equivalent index of the slow light shows giant dispersion near the cut-off wavelength. The layer structure is designed to have a cut-off wavelength of 982 nm, which corresponds to the resonant wavelength for normal incident plane wave in a vertical direction. We calculated the distribution of the electric field amplitude in different wavelengths by using a film-mode-matching method (FIMMWAVE, Photon Design Co.). Fig. 17(b) shows the electric field amplitude distribution during the wavelength tuning of an MEMS VCSEL with a varied air gap [47]. Highly coherent beams are radiated from the surface of the SOA. A change in the radiation angle is as large as 31° for wavelength tuning of 24 nm. A 3-dB saturation power of more than 10 mW with a small-signal gain of 24 dB is predicted for a 1-mm-long SOA. Even if the SOA is driven in the saturation regime, we are able to get a very sharp beam having a divergence angle below 0.1° and an output power of several tens of milliwatts for 1-mm-long SOA. Thus, a large number of resolution points over 300 can be expected for our compact on-chip scanner. The actuation range of the MEMS mirror is 290 nm for a scanning range of 31°. Thus, the required resolution in its displacement is around 1 nm in order to achieve a number of resolution points over 300. While the proposed MEMS approach is not nonmechanical, its tiny structure gives us reasonably high steering speed.

V. CREATION OF A VORTEX BEAM

Optical vortex beams, which have cylindrically symmetric irradiance, helical phase fronts, and an azimuthal component of the wave vector, can carry orbital angular momentum [48].
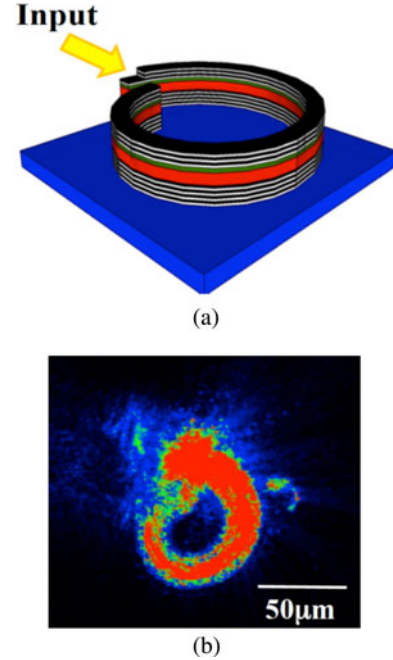
These circularly polarized vortex beams have various unique features and are attracting much attention for various applications such as optical manipulation, optical tweezers, optical imaging, astronomy, quantum information processing, and high-capacity optical communications [49]–[51]. Optical vortex beams have been created by passing Gaussian light beams through optical elements, including computer generated holograms, spiral phase plates, and so on [52]. A recent activity includes compact photonic integrated circuits based on Si-photonics [53]. Here, we propose and demonstrate the creation of vortex beams by using a ring-shaped Bragg reflector waveguide.

Fig. 18(a) shows the schematic structure of an integrated optical vortex beam emitter. The working principle of the angular diffraction element is analogous to that of the straight Bragg reflector waveguide discussed in the previous sections. The wavefront of the radiated light is a plane tilted at angle. If the waveguide is curved to form a loop, the wavefront of the radiated light should skew in the azimuthal direction and hence an optical vortex beam can be created with helical phase fronts and an azimuthal component of the wave vector.

We fabricated a curved Bragg reflector waveguide to form a ring shape with a diameter of 50 μm [54]. The vertical waveguide structure is the same as the passive beam-steering device shown in Section III-B. The waveguide consists of a transparent bulk GaAs core, the 28-pair top DBR, and the 40-pair bottom DBR. The curved waveguide was formed by a standard lithography followed by ICP dry etching. Observed sidewall roughness causes noticeable scattering losses, which could be avoided by the oxidation process used in the straight waveguide in Section III-B. We excited a slow-light mode through a coupling region with a reduced number of the top DBR by using
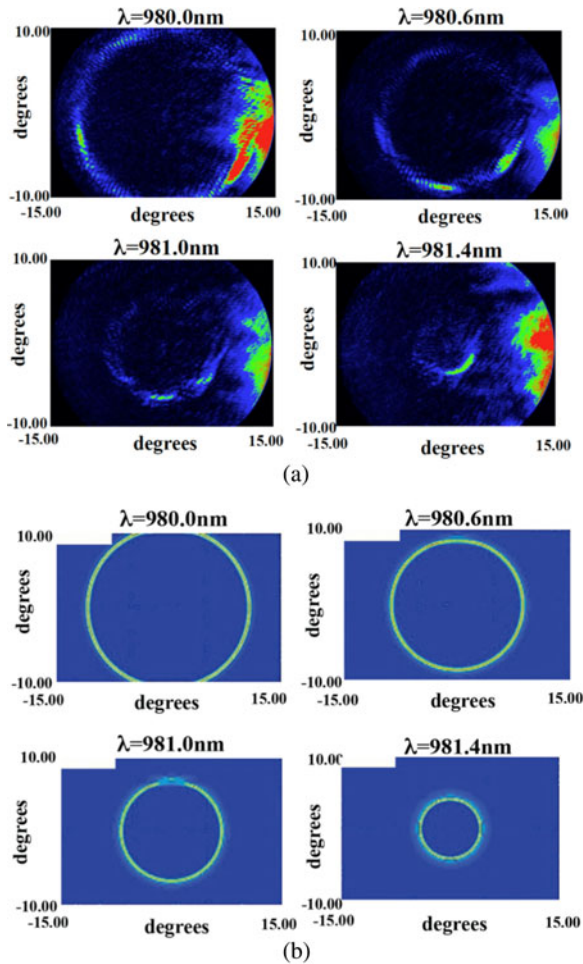
Fig. 19. (a) Measured and (b) calculated FFPs with different wavelengths from 980.0 to 981.4 nm.
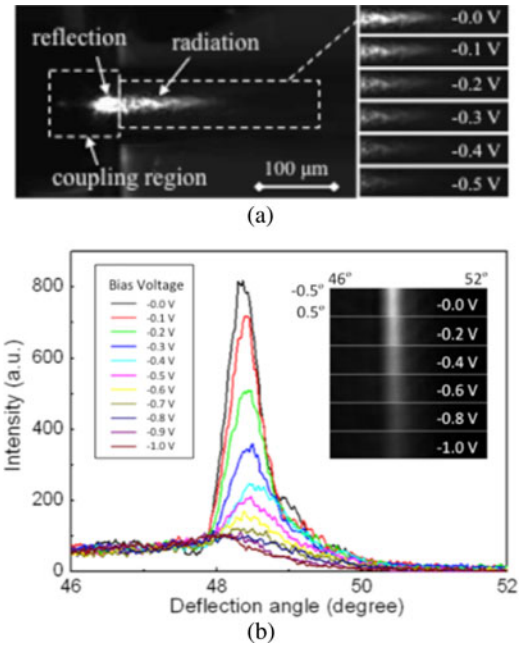

Fig. 20. (a) NFPs with applying different reverse-bias voltages. (b) FFPs and intensity profiles for different bias voltages. The input wavelength is 961 nm.

a tilt-coupling scheme of a lensed fiber in the same way as a straight waveguide. Fig. 18(b) shows the measured NFP. While a scattering loss causes the decay of the intensity along the ring, we could see a circular NFP.

It is noted that the tilt angle of the wavefront of a radiated light is highly dependent on the wavelength and thus can be tuned by changing wavelength. Fig. 19(a) and (b) shows the measured and calculated FFPs with different wavelengths from 980.0 to 981.4 nm. Both are in good agreement. We could observe ring-shaped FFPs with tunable divergence angles. Our vortex emitters can be integrated with a VCSEL for potential applications on mode multiplexing in a multimode fiber.

VI. AMPLITUDE MODULATION IN BEAM STEERING

An optical modulator with low driving voltages is attracting much interest for high-speed operations and low-power consumptions. There have been reports demonstrating modulators with a driving voltage below 1 V [55]–[57]. However, they are always at a cost of either narrow optical bandwidths or long device lengths. Electroabsorption (EA) modulators employing the quantum-confined Stark effect (QCSE) have shown good results in obtaining broad optical bandwidths and high-speed opera-

tion [58]. But there have been difficulties in getting a modulator voltage below 1 V in particular for miniature EA modulators. If we could manage in reducing the light group velocity in EA modulators, QCSE will be significantly enhanced, thanks to the higher light–matter interaction brought by the slowing light effect [34], [35]. The slow-light-induced enhancement enables low driving voltages.

The same device structure shown in Fig. 6 functions as an intensity modulator by applying a reverse-bias voltage in QWs. We demonstrate the additional function of amplitude modulation for beam-steering devices [59]. The device structure measured here is the same as Fig. 6. An input light is coupled through a lensed fiber to the device and propagates along the waveguide. It can promote stronger light–matter interaction inside, thanks to slowing light. The group index is as large as 20, which makes an EA effect larger. If we apply a reverse-bias voltage in QWs, the increased EA due to QCSE decreases the radiated intensity. If we look at the FFP, the radiated intensity is weakened.

NFPs with different bias voltages for a 961-nm input light are shown in Fig. 20(a) [59]. We could observe noticeable change in the radiation pattern (propagation distance) even by a low voltage of only 0.5 V. FFPs and intensity profiles are shown in Fig. 20(b) [59]. A change in the intensity profile is clearly observed. Also, we can see that the deflection angle of the output beam generally keeps constant. Under 0 V bias, the divergence angle is around $0.6°$, which corresponds to a propagation distance of 120–130 μm. An extinction ratio of 5 dB is obtained for a voltage of 0.5 V at 961–963 nm. This voltage is one of the smallest numbers ever reported in compact semiconductor modulators. An extinction ratio of 10 dB can be obtained at a drive voltage below 1 V. The optical bandwidth observed in this experiment has not shown the best performance due to a limitation in laser source tuning range used in the experiment. It may

have a potential to get an optical bandwidth larger than 10 nm for 5 dB modulation under subvolt operations. We could offer the additional function of amplitude modulation with beam steering for use in free-space optical switching and wavelength routing

VII. Conclusion

We present the theoretical basis and beam-steering characteristics of VCSEL-based beam-steering devices. A Bragg reflector waveguide offers large angular dispersion, which is ten times larger than conventional diffraction grating. At the same time, we could get a large FSR of over 100 nm, thanks to its vertical microcavity. The deflection angle of the radiation rotates over $60°$ with tuning the input wavelength and the result well agrees with calculation. By compensating the radiation loss via current injection, the effective propagation length is increased, and hence, the beam divergence is getting narrower below $0.1°$. We also developed a low-loss passive Bragg reflector waveguide composed of transparent materials. A number of resolution points could be scaled up to over 1000 by increasing the effective length in millimeter ranges, which is the highest number in nonmechanical beam-steering devices. We also demonstrated the on-chip integration of a beam-steering function with a VCSEL. In addition, we demonstrate additional functionalities of the creation of vortex beams and the amplitude modulation with beam steering by applying a reverse-bias voltage below 1 V. The result shows a potential of compact and ultrahigh-resolution beam-steering device with N of a few thousands or beyond.

While we focused on a 980-nm wavelength band in this paper, the wavelength band can be flexible by changing layer thicknesses and by choosing suitable materials since there have been a lot of VCSEL activities in a wide spectral range from visible to infrared regions. We see a lot of challenges for future work such as further improvements toward superhigh resolutions, 2-D beam steering, the monolithic integration with a widely tunable VCSEL, high-speed steering via an electro-optic effect, and so on. The proposed concept may open up high-performance beam scanners in sensing and imaging application. Also, we expect a large-scale optical routing and switching building block in compact fashion for DWDM systems.

Acknowledgment

References

[1] J. C. Wyant, "Rotating diffraction grating laser beam scanner," *Appl. Opt.*, vol. 14, pp. 1057–1058, 1975.

[2] T. Matsuda, F. Abe, and H. Takahashi, "Laser printer scanning system with a parabolic mirror," *Appl. Opt.*, vol. 17, pp. 878–884, 1978.

[3] P. F. V. Dessel, L. J. Hornbeck, R. E. Meier, and M. R. Douglass, "A MEMS-based projection display," *Proc. IEEE*, vol. 86, no. 8, pp. 1687–1704, Aug. 1988.

[4] H. H. Refai, J. J. Sluss, and M. P. Tull, "Digital micromirror device for optical scanning applications," *Opt. Eng.*, vol. 46, no. 8, 085401 (5 pp.), 2007.

[5] P. F. McManamon, T. A. Dorschner, D. I. Corkum, L. J. Friedman, D. S. Hobbs, M. Holz, S. Liberman, H. Q. Nguyen, D. P. Resler, R. C. Sharp, and E. A. Watson, "Optical phased array technology," *Proc. IEEE*, vol. 84, no. 2, pp. 268–298, Feb. 1996.

[6] M. T. Johnson and G. S. Seetharaman, "Thermo-optic variable blazed grating for beam steering," *Proc. SPIE*, vol. 6715, no. 1, p. 671505, 2007.

[7] J. Shi, P. J. Bos, B. Winker, and P. F. McManamon, "Switchable optical phased prism arrays for beam steering," *Proc. SPIE*, vol. 5553, no. 1, pp. 102–111, 2004.

[8] O. Pishnyak, L. Kreminska, O. D. Lavrentovich, J. J. Pouch, F. A. Miranda, and B. K. Winker, "Liquid crystal digital beam steering device based on decoupled birefringent deflector and polarization rotator," *Mol. Crys. Liq. Crys.*, vol. 433, pp. 279–295, 2005.

[9] B. Winker, M. Mahajan, and M. Hunwardsen, "Liquid crystal beam directors for airborne free-space optical communications," in *Proc. IEEE Aerospace Conf.*, 2004, vol. 3, pp. 1702–1709.

[10] K. Nakamura, J. Miyazu, M. Sasaura, and K. Fujiura, "Wide-angle, low-voltage electro-optic beam deflection based on space-charge-controlled mode of electrical conduction in KTa1−xNbxO3," *Appl. Phys. Lett.*, vol. 89, no. 13, pp. 131115-1–131115-3, Sep. 2006.

[11] D. R. Scifres, W. Streifer, and R. D. Burnham, "Beam scanning with twin-stripe injection lasers," *Appl. Phys. Lett.*, vol. 33, no. 8, pp. 702–704, Oct. 1978.

[12] S. Mukai, Y. Kaneko, M. Watanabe, H. Itoh, and H. Yajima, "Laser beam scanning using a local deflector integrated with an effective mode filter," *Appl. Phys. Lett.*, vol. 51, no. 25, pp. 2091–2093, Dec. 1987.

[13] N. W. Carlson, G. A. Evans, R. Amantea, S. Palfrey, J. M. Hammer, M. Lurie, L. A. Carr, F. Z. Hawrylo, E. A. James, C. Kaiser, J. B. Kirk, and W. F. Reichert, "Electronic beam steering in monolithic grating-surface-emitting diode laser arrays," *Appl. Phys. Lett.*, vol. 53, no. 23, pp. 2275–2277, Dec. 1988.

[14] Y. Sun, D. A. Francis, S. A. Biellak, A. E. Siegman, and C. J. Chang-Hasnain, "Beam steerable semiconductor lasers with large steering range and resolvable spots," *Electron. Lett.*, vol. 30, no. 24, pp. 2034–2035, 1994.

[15] T. Ide, M. Shimizu, S. Mukai, M. Ogura, T. Kikuchi, Y. Suzuki, R. Kaji, H. Itoh, M. Watanabe, H. Yajima, and T. Nemoto, "Continuous output beam steering in vertical-cavity surface-emitting lasers with two p-Type electrodes by controlling injection current profile," *Jpn. J. Appl. Phys.*, vol. 38, pp. 1966–1970, 1999.

[16] Y. Kurosaka, S. Iwahashi, Y. Liang, K. Sakai, E. Miyai, W. Kunishi, D. Ohnishi, and S. Noda, "On-chip beam-steering photonic-crystal lasers," *Nat. Photon.*, vol. 4, pp. 447–450, 2010.

[17] D. F. Siriani and K. D. Choquette, "Electronically controlled two-dimensional steering of in-phase coherently coupled vertical-cavity laser arrays," *IEEE Photon. Technol. Lett.*, vol. 23, no. 3, pp. 167–169, Feb. 2011.

[18] F. Xiao, W. Hu, and A. Xu, "Optical phased-array beam steering controlled by wavelength," *Appl. Opt.*, vol. 44, pp. 5429–5433, 2005.

[19] K. Van Acoleyen, W. Bogaerts, J. Jágerská, N. Le Thomas, R. Houdré, and R. Baets, "Off-chip beam steering with a one-dimensional optical phased array on silicon-on-insulator," *Opt. Lett.*, vol. 34, no. 9, pp. 1477–1479, 2009.

[20] J. K. Doylend, M. J. R. Heck, J. T. Bovington, J. D. Peters, L. A. Coldren, and J. E. Bowers, "Two-dimensional free-space beam steering with an optical phased array on silicon-on-insulator," *Opt. Exp.*, vol. 19, no. 22, pp. 21595–21604, 2011.

[21] W. Hu and C. Chang-Hasnain, "Optical phased array for far field beam steering with varied HCG," in *Proc. SPIE*, 2012, vol. 8270, 82700H (6 pp.).

[22] X. Gu, T. Shimada, and F. Koyama, "Giant and high-resolution beam steering using slow-light waveguide amplifier," *Opt. Exp.*, vol. 19, no. 23, pp. 22675–22683, Oct. 2011.

[23] F. Koyama, "Recent advances of VCSEL photonics," *IEEE J. Lightw. Technol.*, vol. 24, no. 12, pp. 4502–4513, Dec. 2006.

[24] M. Shirasaki, "Large angular dispersion by a virtually imaged phased array and its application to a wavelength demultiplexer," *Opt. Lett.*, vol. 21, pp. 366–368, 1996.

[25] X. Gu, T. Shimada, A. Fuchida, A. Matsutani, A. Imamura, and F. Koyama, "Beam steering in GaInAs/GaAs slow-light Bragg reflector waveguide amplifier," *Appl. Phys. Lett.*, vol. 99, no. 21, pp. 211107-1–211107-3, Nov. 2011.

[26] X. Gu, T. Shimada, A. Fuchida, A. Matsutani, A. Imamura, and F. Koyama, "Ultra-compact beam-steering device based on Bragg reflector waveguide amplifier with number of resolution points over 100," *Electron. Lett.*, vol. 48, no. 6, pp. 336–337, Mar. 2012.

[27] X. Gu, T. Shimada, A. Fuchida, A. Matsutani, A. Imamura, and F. Koyama, "Electro-thermal beam steering using Bragg reflector waveguide amplifier," *Jpn. J. Appl. Phys.*, vol. 51, 020206 (3 pp.), Feb. 2012.

[28] X. Gu, T. Shimada, A. Matsutani, and F. Koyama, "Miniature non-mechanical beam deflector based on Bragg reflector waveguide with a number of resolution-points larger than 1,000," *IEEE Photon. J.*, vol. 4, no. 5, pp. 1712–1719, Oct. 2012.

[29] D. R. Wisely, "32 channel WDM multiplexer with 1-nm channel spacing and 0.7-nm bandwidth," *Electron. Lett.*, vol. 27, pp. 520–521, 1991.

[30] T. Shimada, A. Matsutani, and F. Koyama, "On-chip electro-thermal beam steering based on slow-light Bragg reflector waveguide laterally integrated with VCSEL," in *Proc. IEEE Photon. Conf.*, Sep. 2012, pp. 244–245.

[31] P. Yeh, A. Yariv, and E. Marom, "Theory of Bragg Fiber," *J. Opt. Soc. Amer.*, vol. 68, pp. 1196–1201, 1978.

[32] Y. Sakurai and F. Koyama, "Control of group delay and chromatic dispersion in tunable hollow waveguide with highly reflective mirrors," *Jpn. J. Appl. Phys.*, vol. 8B, pp. 5828–5833, 2004.

[33] G. Hirano, F. Koyama, K. Hasebe, T. Sakaguchi, N. Nishiyama, C. Caneau, and C.-E. Zah, "Slow light modulator with Bragg reflector waveguide," in *Proc. Opt. Fiber Commun. Conf.*, Anaheim, CA, USA, 2007, pp. 25–29, Paper DP34.

[34] T. F. Krauss, "Why do we need slow light?," *Nat. Photon.*, vol. 2, pp. 448–450, 2008.

[35] Z. Shi, R. W. Boyd, D. J. Gauthier, and C. C. Dudley, "Enhancing the spectral sensitivity of interferometers using slow-light media," *Opt. Lett.*, vol. 32, pp. 915–917, 2007.

[36] L. Thevenaz, "Slow and fast light in optical fibres," *Nat. Photon.*, vol. 2, pp. 474–481, 2008.

[37] T. F. Krauss, "Slow light in photonic crystal waveguides," *J. Phys. D, Appl. Phys.*, vol. 40, pp. 2666–2670, 2007.

[38] E. Mizuta, H. Watanabe, and T. Baba, "All semiconductor low-Δ photonic crystal waveguide for semiconductor optical amplifier," *Jpn J. Appl. Phys.*, vol. 45, pp. 6116–612, 2006.

[39] A. Fuchida, A. Matsutani, and F. Koyama, "Slow-light total-internal- reflection switch with bending angle of 30 deg," *Opt. Lett.*, vol. 36, pp. 2644–2646, 2011.

[40] T. Miura and F. Koyama, "Novel phase-tunable three-dimensional hollow waveguides with variable air core," *IEEE Photon. Technol. Lett.*, vol. 15, no. 9, pp. 1240–1242, Sep. 2003.

[41] A. S. Sudbo, "Film mode matching: a versatile numerical method for vector mode field calculations in dielectric waveguides," *Pure Appl. Opt.*, vol. 2, pp. 211–233, 1993.

[42] M. T. Johnson, D. F. Siriani, J. D. Sulkin, and K. D. Choquette, "Phase and coherence extraction from a phased vertical cavity laser array," *Appl. Phys. Lett.*, vol. 101, 031116 (3 pp.), 2012.

[43] X. Gu, T. Shimada, A. Matsutani, and F. Koyama, "High-resolution wavelength demultiplexer based on a Bragg reflector waveguide amplifier with large angular dispersion," presented at the Eur. Conf. Exhib. Opt. Commun., Mo.2.E, Amsterdam, The Netherlands, 2012.

[44] T. Shimada and F. Koyama, "Lateral integration of VCSEL with slow light amplifier/modulator," in *Proc., 23rd Annu. Meeting IEEE Photon. Soc.*, 2010, pp. 244–245.

[45] T. Shimada, A. Matsutani, and F. Koyama, "On-chip electro-thermal beam steering based on slow-light Bragg reflector waveguide laterally integrated with VCSEL," in *Proc. IEEE Photon. Conf.*, 2012, pp. 244–245.

[46] C. J. Chang-Hasnain, "Tunable VCSELs," *IEEE. J. Sel. Topics Quantum Electron.*, vol. 6, no. 6, pp. 978–987, Nov.–Dec. 2000.

[47] M. Nakahama, X. Gu, T. Shimada, and F. Koyama, "On-hip high-resolution beam scanner based on Bragg reflector slow-light waveguide amplifier and tunable micro-electro-mechanical system vertical cavity surface emitting laser," *Jpn. J. Appl. Phys.*, vol. 51, 040208 (3 pp.), Mar. 2012.

[48] L. Allen, M. W. Beijersbergen, R. J. C. Spreeuw, and J. P. Woerdman, "Orbital angular momentum of light and the transformation of Laguerre-Gaussian laser modes," *Phys. Rev. A*, vol. 45, pp. 8185–819, 1992.

[49] D. G. Grier, "A revolution in optical manipulation," *Nature*, vol. 424, pp. 810–816, 2003.

[50] A. Mair, A. Vaziri, G. Weihs, and A. Zeilinger, "Entanglement of the orbital angular momentum states of photons," *Nature*, vol. 412, pp. 313–316, 2001.

[51] J. Wang, J. Y. Yang, I. M. Fazal, N. Ahmed, Y. Yan, H. Huang, Y. Ren, Y. Yue, S. Dolinar, M. Tur, and A. E. Willner, "Terabit free-space data transmission employing orbital angular momentum multiplexing," *Nat. Photon.*, vol. 6, pp. 488–496, 2012.

[52] N. R. Heckenberg, R. McDuff, C. P. Smith, and A. G. White, "Generation of optical phase singularities by computer-generated holograms," *Opt. Lett.*, vol. 17, pp. 221–223, 1992.

[53] X. Cai, J. Wang, M. J. Strain, B. Johnson-Morris1, J. Zhu, M. Sorel, J. L. O'Brien, M. G. Thompson, and S. Yu, "Integrated compact optical vortex beam emitters," *Science*, vol. 338, no. 6105, pp. 363–366, 2012.

[54] S. Mochizuki, X. Gu, T. Shimada, A. Matsutani, and F. Koyama, "Control of far-field patterns from slow-light amplifier," in *JSAP Meeting*, 13p-C5-11, 2012.

[55] Y. Shi, C. Zhang, H. Zhang, J. H. Bechtel, L. R. Dalton, B. H. Robinson, and W. H. Steier, "Low (sub-1-volt) halfwave voltage polymeric electro-optic modulators achieved by controlling chromophore shape," *Science*, vol. 288, pp. 119–122, 2000.

[56] N. C. Helman, J. E. Roth, D. P. Bour, H. Altug, and D. A. B. Miller, "Misalignment-tolerant surface-normal low-voltage modulator for optical interconnects," *IEEE J. Sel. Topics Quantum Electron.*, vol. 11, no. 2, pp. 338–342, Mar.–Apr. 2005.

[57] S. Manipatruni, K. Preston, L. Chen, and M. Lipson, "Ultra-low voltage, ultra-small mode volume silicon microring modulator," *Opt. Exp.*, vol. 18, no. 17, pp. 18235–18242, 2010.

[58] T. Ido, H. Sano, D. J. Moss, S. Tanaka, and A. Takai, "Strained In-GaAs/InAlAs MQW electroabsorption modulators with large bandwidth and low driving voltage," *IEEE Photon. Technol. Lett.*, vol. 6, no. 10, pp. 1207–1209, Oct. 1994.

[59] X. Gu, T. Shimada, S. Shimizu, A. Matsutani, and F. Koyama, "Compact Bragg reflector waveguide modulator based on VCSEL structure with low driving voltage below 0.5 V," in *Proc. 23rd IEEE Int. Semiconductor Laser Conf.*, 2012, pp. 124–125, TuP26.

Fumio Koyama (F'08) received the B.S., M.S., and Ph.D. degrees in physical electronics from the Tokyo Institute of Technology, Tokyo, Japan, in 1980, 1982, and 1985, respectively.

He is a Professor of the Photonics Integration System Research Center, P&I Lab., Tokyo Institute of Technology, and has served as an Adjunct Distinguished Professor at King Abdulaziz University, Jeddah, Saudi Arabia. He is currently doing research on VCSELs, photonic-integrated WDM devices, optical MEMS devices, and related semiconductor microfabrication technologies. From 1992 to 1993, he was with AT&T Bell Labs, Crawford Hill, as a Visiting Researcher. He has authored or coauthored more than 380 journal papers and 400 conference papers, including 60 invited papers. He is one of ISI's highly cited researchers.

Dr. Koyama received the IEEE Student Paper Award in 1985, the IEE Electronics Letters Premium in 1985 and in 1988, the Paper Awards from the IEICE of Japan in 1990, 2002, 2004, and 2007, the excellent review paper award from the Japan Society of Applied Physics in 2000, the Marubun Scientific Award from the Marubun Research Promotion Foundation in 1998, the Ichimura Award from the New Technology Development Foundation in 2004, the Electronics Society Award from the IEICE of Japan in 2006, the Prize for Science and Technology from the Minister of Education, Culture, Sports, Science and Technology in 2007, the IEEE/LEOS William Streifer Scientific Achievement Award in 2008, the Micro-Optics award in 2011, and the Izuo Hayashi Award from the Japan Society of Applied Physics in 2012. He is Fellow of the Institute of Electrical, Information and Communication Engineers and the Japan Society of Applied Physics.

Xiaodong Gu (S'12) received the B.S. degree in optical engineering from Zhejiang University, Hangzhou, China, in 2010 and the M.S. degree in electronics and applied physics from the Tokyo Institute of Technology, Yokohama, Japan, in 2012. He is currently working toward the Ph.D. degree in electronics and applied physics under Prof. F. Koyama at the Tokyo Institute of Technology.

His current research focuses on functional photonics devices, e.g., beam scanners, switches, and modulators. His research interests include optical interconnects and biophotonics.